Fuel 137 (2014) 77–84

Contents lists available at ScienceDirect

Fuel

journal homepage: www.elsevier.com/locate/fuel

Key thermal events during pyrolysis and CO_2-gasification of selected combustible solid wastes in a thermogravimetric analyser

Tianju Chen [a], Jingli Wu [a], Zhezi Zhang [b], Mingming Zhu [b], Li Sun [a], Jinhu Wu [a,b,*], Dongke Zhang [a,b,*]

[a] Key Laboratory of Biofuels, Qingdao Institute of Bioenergy and Bioprocess Technology, Chinese Academy of Sciences, 189 Songling Road, Qingdao 266101, PR China
[b] Centre for Energy (M473), The University of Western Australia, 35 Stirling Highway, Crawley, WA 6009, Australia

HIGHLIGHTS

- Pyrolysis and gasification of representative combustible solid wastes were studied.
- Three generic characteristic thermal events were identified during CO_2-gasification.
- Occurrence of the key thermal events depends on the material type and properties.
- CO_2-gasification kinetics was obtained in different stages of the conversion.

ARTICLE INFO

Article history:
Received 6 April 2014
Received in revised form 17 July 2014
Accepted 24 July 2014
Available online 5 August 2014

Keywords:
Combustible solid waste
Gasification
Kinetics
Pyrolysis
Thermogravimetric analyser

ABSTRACT

Key characteristic thermal events during the pyrolysis and CO_2-gasification of six representative combustible solid wastes (CSWs), namely, poplar, paper, polyethylene (PE), rubber, dacron and rice, were investigated using a thermogravimetric analyser (TGA) in order to observe and contrast the thermal behaviour of these materials during pyrolysis and gasification and as a means to reveal their thermal conversion mechanisms. The TGA experiments were carried out in N_2 and CO_2 atmospheres, respectively, and from room temperature to 1193 K at various heating rates ranging from 5 to 30 K min^{-1}. Three generic characteristic thermal events, namely, pyrolysis of the raw CSW (stage I), gasification of the char of incomplete carbonisation (stage II), and gasification of the fixed carbon (stage III), were identified during the CO_2 gasification processes. It was observed that the poplar and paper samples went through all the three key events, however, the PE and rice samples only incurred stage I, while the rubber and dacron samples only showed the stages I and III events. In addition, the pyrolysis process (stage I) of all six CSW samples during the CO_2-gasification was similar to that in N_2 but, as expected, the reaction was shifted to occur at slightly higher temperatures in CO_2. The activation energy of the CO_2-gasification reactions in the different stages of conversion was estimated from the TGA data using the Friedman iso-conversional method. The activation energy for the pyrolysis of poplar, PE and dacron remained relatively constant while that for paper, rice and rubber increased with increasing the degree of conversion in stage I.

1. Introduction

Combustible solid wastes (CSWs) such as kitchen garbage, paper, textile, wood, leather, plastics and garden waste can be utilised in various waste-to-energy processes to recover energy in form of electricity, gaseous or liquid fuels, and steam for heating, while the final volume of the waste to be disposed of is minimised. Waste-to-energy is recognised as a renewable energy technology and is increasingly playing an important role in the CSW management [1].

There are extensive studies in the literature on waste-to-energy of CSW using various thermochemical conversion technologies, such as combustion [2,3], pyrolysis [4] and gasification [5]. Incineration (combustion), often incorporating a steam cycle for power generation, is a well-established and dominant process of municipal solid waste (MSW) disposal. In the process of incineration, there are major concerns over persistent organic pollutants (POPs),

* Corresponding authors. Address: Key Laboratory of Biofuels, Qingdao Institute of Bioenergy and Bioprocess Technology, Chinese Academy of Sciences, 189 Songling Road, Qingdao 266101, PR China. Tel.: +86 532 80662761 (J. Wu). Address: Centre for Energy (M473), The University of Western Australia, 35 Stirling Highway, Crawley, WA 6009, Australia. Tel.: +61 8 6488 7600 (D. Zhang).
E-mail addresses: wujh@qibebt.ac.cn (J. Wu), Dongke.Zhang@uwa.edu.au (D. Zhang).

http://dx.doi.org/10.1016/j.fuel.2014.07.077
0016-2361/

such as polychlorodibenzo-p-dioxins (PCDDs) and polychlorodibenzo furans (PDCFs) [6]. PCDD/Fs are almost always formed as undesired by-products during the combustion of CSW when chlorine, oxygen, hydrogen and carbon are present [7,8]. Against the aforementioned backdrops, gasification of CSW in steam and/or CO_2 offers several potential benefits over the conventional approach of incineration of CSW [9]. The most significant one is the reduction of the emissions of corrosive and toxic compounds due to low operating temperatures and reducing conditions [10]. The syngas produced from the gasification process can be cleaned and combusted in conventional burners, reciprocating engines or gas turbines, for combined heat and power generation. In addition, its main components, carbon monoxide and hydrogen, can also offer the basic building blocks for producing valuable products [9,11]. However, one of the significant operational challenges is that the nature and composition of the CSW major components are highly variable, which directly affect the gasification plant of given design. Better understanding of the gasification behaviour of a given CSW feedstock is essential for reactor design, plant operation and optimisation [5]. Among a number of laboratory approaches, the non-isothermal thermogravimetric analysis (TGA) is one of the most commonly used thermoanalytical techniques for CSW gasification studies [5,12,13], in which the experiments can be performed in a well-controlled manner. The data obtained from the TGA experiments can be utilised to determine the kinetics of CSW gasification by using the isoconversional methods [14].

In the previous research, the liquid production from the pyrolysis of biomass [15,16] and sewage sludge [17,18] were investigated. The present contribution reports a non-isothermal TGA study of the pyrolysis in N_2 and CO_2-gasification of six representative CSW samples, aiming to identify the key thermal events during the CSW gasification process. Activation energy was also obtained by applying the Friedman iso-conversional technique to process the TGA experimental data. It was anticipated that the outcomes of this study would provide some new insights into the gasification processes of different CSW and their differences.

2. Experimental

2.1. Materials

Six representative samples, namely, poplar woodchips, used printing paper, rice, polyethylene (PE), dacron (a synthetic polyester fibre) and spent tyre, were chosen for this study because they represent six typical combustible solid wastes (CSWs), namely biomass, papers, kitchen garbage, plastics, textiles and rubbers, respectively. In order for the results to be of general relevance and significance with no influence of contaminations, all samples were collected from clean sources in the present experimentation. The proximate and ultimate analyses of the samples are listed in Table 1. Prior to the experiment, the samples were dried in an electrically heated oven at the temperature of 378 K for 12 h and stored in air-tight bags until experimentation.

Table 1
The proximate and ultimate analyses of the six typical CSW samples.

	Poplar	Paper	Rice	PE	Dacron	Rubber
Proximate analysis[a] *(wt.%)*						
Volatiles	79.55	79.35	84.42	99.98	75.24	62.83
Fixed carbon	20.05	9.98	15.18	0.02	24.61	26.93
Ash	8.11	10.66	0.40	0	0.14	10.23
HHV (MJ/kg)	16.08	11.67	15.06	44.09	28.31	34.16
Ultimate analysis[b] *(wt.%)*						
Nitrogen	1.16	0.05	1.48	0	22.05	0.51
Carbon	46.67	36.08	40.76	85.66	65.58	79.9
Hydrogen	5.74	4.82	6.46	14.08	5.48	6.76
Sulfur	0.09	0.1	0.2	0.26	0.35	1.59
Oxygen[c]	46.34	58.95	51.1	0	6.54	–

[a] Dry basis.
[b] Dry and ash free basis.
[c] By difference.

2.2. Experimental procedures

The experiments were performed using a thermogravimetric analyser (TGA, TA Instruments Q5000IR), operating at four different heating rates, namely 5, 10, 20 and 30 K min^{-1}, respectively. These heating rates were chosen in such a way that they were slow enough to allow isothermal experience of the whole sample during the TGA experiments, yet they would allow kinetic analysis using the Friedman isoconversional method [19]. A thin layer of the sample (ca. 10 mg) was distributed evenly in a ceramic crucible and placed in the TGA. The sample was then heated at a desired heating rate to the final temperature of 1193 K. The reaction of such a thin layer of sample could be considered kinetically controlled without incurring any significant mass and heat transfer limitations of concern [20]. During the heating, the mass and temperature of the sample were simultaneously and continuously recorded. In the pyrolysis experiments, N_2 of ultra high purity was passed through the TGA at a constant flow rate of 100 mL min^{-1} to provide the inert gas environment and to sweep away the volatile released. In the gasification experiments, a mixture of 80% CO_2 and 20% N_2, both of ultra high purity was used at a constant flow rate of 100 mL min^{-1}.

2.3. Kinetic analysis using the Friedman method

The TGA data of the pyrolysis and CO_2-gasification of the selected CSW components in this work were subjected to kinetic analysis using the Friedman method [19] as a means to compare the characteristics of these different materials during the thermal processing. The single step reaction model is commonly used for pyrolysis and gasification studies [21,22] as it is independent of the heating rate to estimate the reaction kinetics. The rate of solid-state degradation or conversion, $d\alpha/dT$, can be described by

$$\frac{d\alpha}{dT} = \frac{1}{\beta}k(T)f(\alpha) = \frac{1}{\beta}A\exp\left(\frac{-E}{RT}\right)f(\alpha) \quad (1)$$

where α is the degree of conversion, T the particle temperature (K), β the linear heating rate (K min^{-1}) in the TGA experiment, $k(T)$ the temperature-dependent rate constant, $f(\alpha)$ the differential conversion function, A the pre-exponential factor (min^{-1}), E the activation energy (kJ mol^{-1}) and R is the universal gas constant (8.314 JK^{-1} mol^{-1}), respectively.

The degree of conversion, α, is determined from Eq. (2).

$$\alpha = \frac{m_i - m_t}{m_i - m_f} \quad (2)$$

where m_i is the initial mass, m_t the mass at time t, and m_f is the final mass.

Rearranging Eq. (1) into a logarithmic form using the Friedman method [19] leads to

$$\ln\left[\beta\left(\frac{d\alpha}{dT}\right)_a\right] = \ln\left[A_\alpha, f(\alpha)\right] - \frac{E_\alpha}{RT_\alpha} \quad (3)$$

For a given value of the degree of conversion, the plot of $\ln[\beta(d\alpha/dT)$ vs. $1/T_\alpha$ should be a straight line with the slope being $-E_\alpha/R$, from which the activation energy can be calculated.

3. Results and discussion

3.1. Thermogravimetric analysis

Fig. 1(a–f) shows the thermogravimetric (TG) and derivative thermogravimetric (DTG) curves of the six CSW components in both N_2 and CO_2 atmospheres at a heating rate of 10 K min^{-1}. As shown in Fig. 1(a), the pyrolysis of the poplar wood sample in N_2 started at 400 K, reaching a maximum rate of mass loss at 612 K. As the temperature continued to increase, the mass loss rate decreased and the mass became invariant when the temperature was higher than 800 K, indicating the completion of the pyrolysis process. This is consistent with the literature findings that there are two pyrolysis regions for lignocellulosic biomass, namely the active and passive pyrolysis [23–25]. The decomposition of hemicellulose and cellulose mainly occur in the active pyrolysis region, while the decomposition of lignin starts in the later part of the active pyrolysis region and completes in the passive pyrolysis region without the characteristic peaks of the other two major biomass components. For the CO_2-gasification experimental curves shown in Fig. 1(a), at temperatures below 800 K, the general trend of the weight change in CO_2 was similar to that in N_2 although the TG and DTG curves in CO_2 shifted to a higher temperature region by ca 10 K relative to N_2. This suggests that the poplar underwent a similar pyrolysis process in the CO_2 atmosphere to that in N_2 at low temperatures which were insufficient to cause the CO_2-gasification reaction of the poplar. In the meantime, CO_2 has a lower heat capacity than N_2 at temperatures lower than 600 K, less heat was removed from the sample by CO_2 and therefore, the small temperature shift. However, significant additional weight loss was evident at temperatures above 900 K in CO_2, indicating the CO_2 gasification reactions with the remaining char and fixed-carbon as shown in Eqs. (4) and (5), respectively, had occurred [5].

$$CH_mO_n + CO_2 \rightarrow CO + H_2O \quad (4)$$

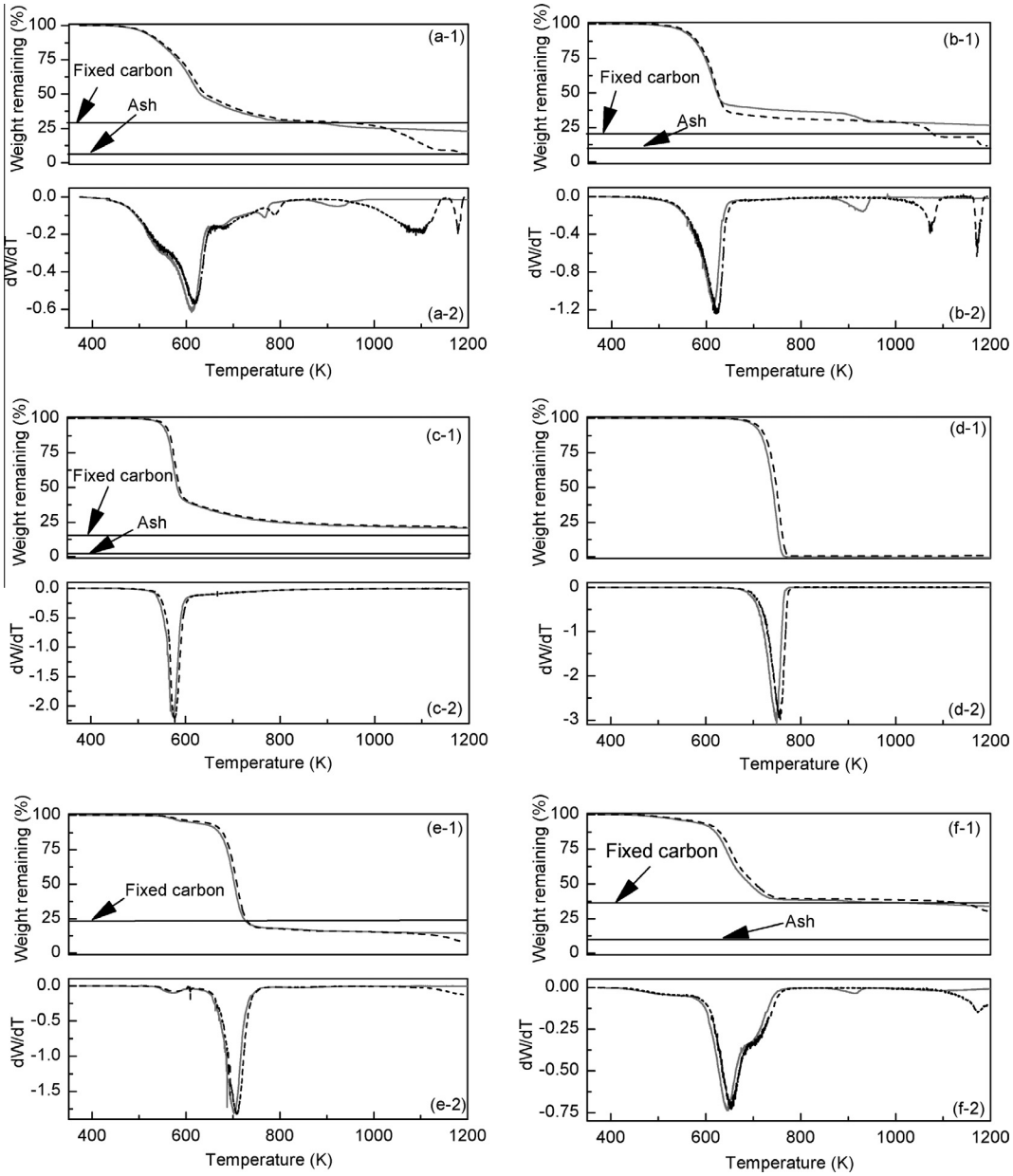

Fig. 1. The TG (-1) and DTG (-2) curves of the six typical CSW components in both N_2 (solid lines) and CO_2 (dashed lines) atmospheres at a heating rate of 10 K min^{-1}: (a) Poplar, (b) Paper, (c) Rice, (d) PE, (e) Dacron, and (f) Rubber.

$$C + CO_2 \rightarrow 2CO + 173.5\ kJ\ mol^{-1} \quad (5)$$

The char produced from the pyrolysis still contained a noticeable amount of volatile matter (and the presence of hydrogen and oxygen) due to incomplete carbonisation in the pyrolysis process, which would promote the gasification reaction of the carbon complex of the remaining char with CO_2, as described in Eq. (4) [15,16]. With further increases in temperature, hydrogen and oxygen related compounds would be gradually squeezed out of the matrix of the char, resulting in an increase in the fixed carbon content in the remaining carbonaceous material [26]. As the temperature further increased, the reaction between CO_2 and the fixed carbon, described in Eq. (5), inevitably became dominant. Similar results can be found for the paper, which mainly consists of hemicellulose and cellulose, as shown in Fig. 1(b). The maximum rates of weight losses during pyrolysis of both poplar wood and paper occurred at ca 612 K, which was almost identical to that of cellulose pyrolysis under the same condition from our previous studies [27]. The positions of the DTG peaks in the gasification region for paper and poplar wood in CO_2 atmosphere occurred at ca 1084 K and ca 1089 K, respectively. Fig. 1(b-2) shows a peak (at 900 K), in addition to the peak at 620 K, appeared in the nitrogen atmosphere but not in CO_2, due to the different reactions incurred: in pyrolysis, the two peaks are due to the thermal decomposition of cellulose (at ca. 620 K) and hemicellulose (at ca. 900 K); but in CO_2 gasification, CO_2 attacks both C–C and C–H bonds indiscriminately [15–17,27] and therefore only the peak at 620 K was observed. Fig. 1(c) illustrates the thermal decomposition behaviour of the rice in both N_2 and CO_2 atmospheres. It can be seen that the major weight loss of the rice occurred at 500–615 K with the maximum rate of weight loss at 573 K in N_2 and 577 K in CO_2. The DTG curves in Fig. 1(c-2) show that the flat tailing sections in both N_2 and CO_2 atmospheres above ca 615 K fell into the same line. It is speculated that the solid residues from the pyrolysis of rice consisting mainly of carbohydrates, had very low gasification reactivity in the temperature range studied. Therefore, no gasification reaction occurred for the rice.

The TG and DTG curves in Fig. 1(d) show the thermal decomposition behaviour of the PE sample in both N_2 and CO_2 atmospheres, respectively. Clearly, all the materials decomposed between ca 650 K and 785 K leaving literally no solid residue behind and with a single DTG peak for both conditions. The maximum rate of pyrolysis in N_2 occurred at a temperature only ~8 K lower than that in CO_2 at ca 765 K, suggesting that little or no CO_2-gasification reaction of PE during and after the pyrolysis.

The thermal decomposition behaviour of dacron is shown in Fig. 1(e). The weight loss curves in CO_2 and N_2 deviated at ca 1015 K, indicating that the CO_2-gasification reaction of the solid residues had started. Before the commencement of the gasification, dacron underwent a similar pyrolysis process in CO_2 to that in N_2. A minor pyrolysis peak in the temperature range of 530–600 K followed by a major peak in the temperature range of 600–780 K were observed from the DTG curves as shown in Fig. 1(e-2). However, the maximum rate of pyrolysis in CO_2 was shifted to the higher temperature region by ca 6 K, as in all other cases.

Fig. 1(f) shows the TGA results of rubber in CO_2 and N_2. Similar to dacron, the CO_2-gasification of the rubber occurred at temperatures higher than 1080 K with a minor pyrolysis peak in the temperature range of 473–550 K followed by a major weight loss in the temperature range of 550–780 K.

In Fig. 1, small peaks at the temperature of 900 K during pyrolysis and some peaks between 1000 K and 1200 K during CO_2-gasification process are evident in (a-2), (b-2) and (f-2) but not in (c-2), (d-2) and (e-2). These differences in the thermal behaviour during pyrolysis and CO_2-gasification of the six materials are attributed to their different compositions and the different chemical bonds involved in each of the components of them. The thermal behaviour of the poplar and paper samples resembled the characteristics of cellulose, hemicellulose and lignin, which have several distinctly different types of chemical bonds and, as such, the various peaks were observed in the DTG curves of these two samples. The same was not seen for the rice, PE and Dacron samples as they are of narrow ranges of chemical bonds, respectively, that is, carbohydrates for rice and unique polymers for both PE and Dacron and their thermal decomposition behaviours are expected to be unique and simple. In CO_2-gasification, the porous structures of the chars formed during the gasification of the poplar, paper and rubber samples also play an important role in determining the thermal mass loss behaviour and therefore the additional peaks observed.

An inspection of all the TGA results for the six representative CSW components suggests that the gasification behaviour of these CSW materials in CO_2 were distinctly different in several ways. In the temperature range studied, three characteristic reaction stages can be identified from the TGA results of the gasification of poplar wood and paper, both of lignocellulose nature, namely pyrolysis stage (stage I), gasification of the char of incomplete carbonisation (stage II) and the gasification of the fixed carbon (stage III). These reaction stages were defined according to the features on the DTG curves. When a DTG peak receded back to zero, the corresponding reaction stage was considered to have completed. The thermal decomposition behaviour of rice was almost identical in both N_2 and CO_2 and only incurred the pyrolysis stage (stage I). Likewise, PE also only showed the stage I pyrolysis reactions and was of the least thermal stability among all the six CSW samples studied with complete decomposition occurring before 785 K during the CO_2-gasification process. Only two reaction stages were observed for dacron and rubber when reacted with CO_2. The pyrolysis stage completed at ca 780 K for both materials while the gasification reactions started at 1015 K and 1080 K, respectively.

The fixed carbon and ash contents of the representative CSW samples, as determined by the proximate analysis, are also respectively marked in Fig. 1 for comparison and bench-marking. Fig. 1(b, e and f) shows that for the paper, dacron and rubber samples, the CO_2-gasification reactions continued to below the fixed carbon lines, supporting the fixed carbon gasification theory in the stage III. The fixed carbon and ash contents of the PE sample were practically zero and therefore no stage III reaction was observable. However, for the poplar sample, the stages II and III reactions proceeded from above to below its fixed carbon line. Generally speaking, the hemicellulose incurs thermal decomposition at 423–623 K, the cellulose degradation appears between 548 and 623 K and the lignin degradation takes place at 473–973 K [27]. Thus, it is believed that in the present work, the biochar of the poplar sample reacted in stage II, and the fixed carbon in stage III with CO_2. For the rice sample, however, the weight remaining at 1200 K was greater than the fixed carbon line, suggesting that the CO_2-gasification reactions were not dominating before the temperature reached 1200 K [28]. Note that the starch in rice incurred the stage II reaction at 1200–1400 K.

The TG and DTG curves obtained from the gasification of the typical CSW samples in CO_2 at different heating rates (β: 5, 10, 20 and 30 K min^{-1}) are shown in Fig. 2. Clearly, the heating rate affected the positions of TG and DTG curves and the maximum decomposition rate. This can be explained that the sample reacting at a higher heating rate experienced a shorter reaction time and therefore the temperature needed for the sample to achieve the same degree of conversion was also higher [23]. In order to better understand the gasification process, the key thermal events of each stage of the CSW gasification in CO_2 heated at different heating rates are described by the characteristic temperatures, namely the initiating temperature (T_i), peak temperature (T_p) and completion temperature (T_f) as summarised in Table 2.

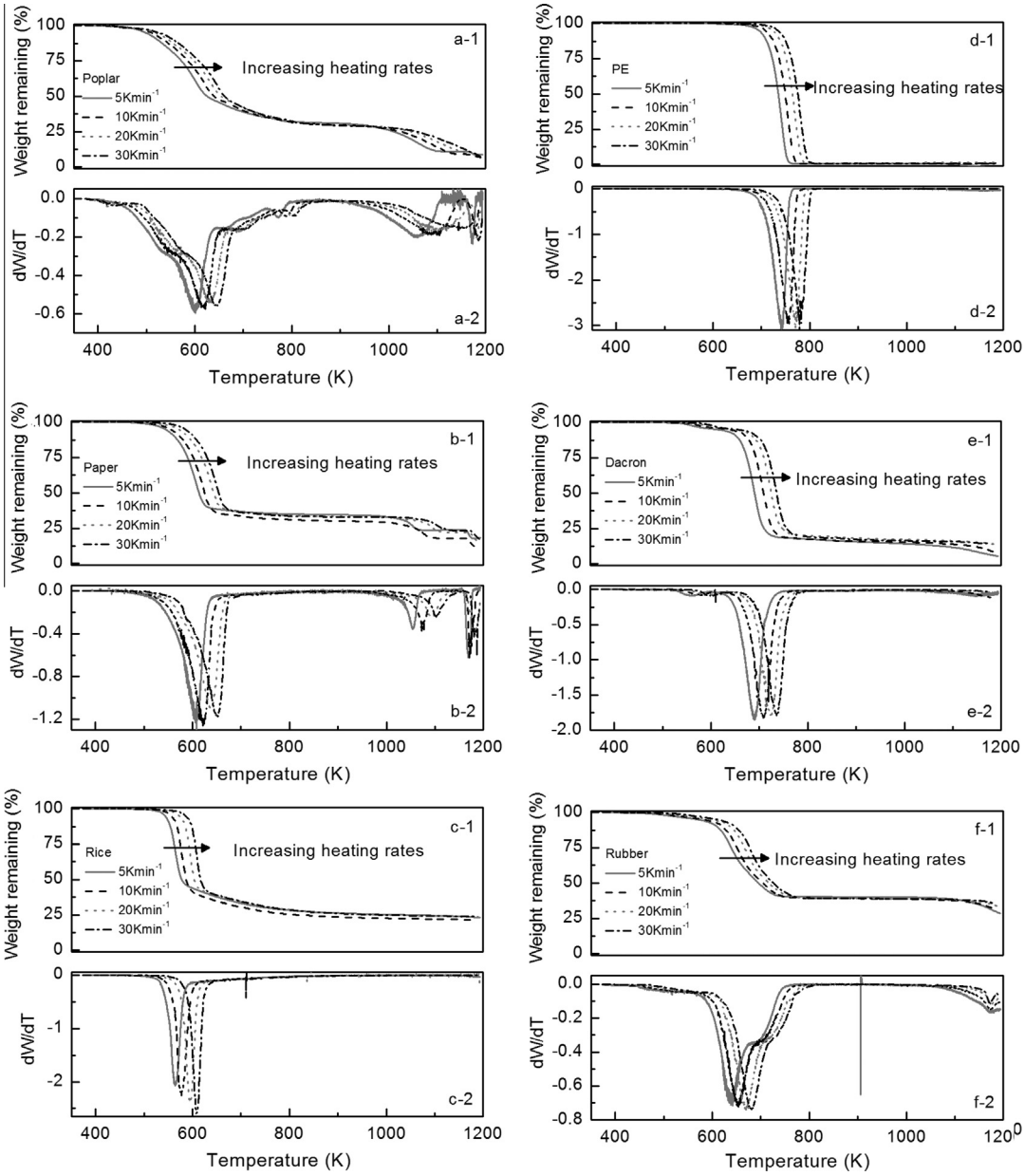

Fig. 2. The TG (-1) and DTG (-2) curves of the six typical CSW components in CO_2 at different heating rates: (a) Poplar, (b) Paper, (c) Rice, (d) PE, (e) Dacron, and (f) Rubber.

3.2. Kinetic analysis

The TGA data were analysed according to the Friedman method to determine the model-free activation energy. Fig. 3 shows the conversion vs. temperature plots of the reaction stages I and II, respectively, of the CO_2-gasification of poplar as an example. Unfortunately, due to the instrument limitation in the final gasification temperature, the reaction stage III of both poplar and paper were not completed in the present studies. Thus, the kinetic analysis were only performed in the reaction stages I and II. Fig. 4 shows the plot of the natural logarithm of the left hand side of Eq. (3) against $1/T$ as a function of conversion from 0.15 to 0.85. The model-free activation energy at each conversion was obtained from the slope of the linear regression line in Fig. 4. The calculated squares of the correlation coefficient, R^2, corresponding to the linear fitting used in the Friedman method were in the range from 0.98 to 1. The calculated activation energy as a function of conversion is presented in Fig. 5. Note that for all materials studied, the activation energy did not remain constant but changed as the reaction proceeded during pyrolysis and CO_2-gasification processes. This is expected as the materials were not pure compounds but a mixture of different components with complex chemical bonding structures. It is also evident that the changes of the activation energy as a function of conversion of the six materials behaved differently as the composition and chemical structures of the six materials studied varied so significantly. The change in the activation energy as a function of conversion determined in the reaction stages I and II for paper had a very similar trend to that for poplar but with slightly higher values than that of poplar. This is reasonable as both materials consisted of cellulose, hemicellulose and lignin. It is also noted that the activation energies in stage II of both paper and poplar increased as the conversion increased till 50% and then decreased when the conversion was greater than 50%. With the progress of carbonisation in stage II, the volatile matter or hydrocarbon molecules remaining in the biochar continued to decompose and the carbon structure became more ordered as

Table 2
Characteristic temperatures of the key thermal events identified during the pyrolysis and CO_2-gasification of the six typical CSW samples.

Sample	Heating rate ($K\,min^{-1}$)	Key thermal events								
		Stage I			Stage II			Stage III		
		T_i (K)	T_p (K)	T_f (K)	T_i (K)	T_p (K)	T_f (K)	T_i (K)	T_p (K)	T_f (K)
Poplar	5	418	601	808	808	1064	1119	1119	1173	1193
	10	438	616	823	823	1094	1154	1154	1178	Incomplete
	20	455	631	864	864	1115	1166	1166	1182	Incomplete
	30	477	636	859	859	1156	1171	1171	1183	Incomplete
Paper	5	442	608	904	904	1055	1087	1087	1170	1193
	10	440	623	901	901	1073	1094	1094	1173	Incomplete
	20	472	640	929	929	1095	1127	1127	1182	Incomplete
	30	464	651	954	954	1103	1148	1148	1184	Incomplete
Rice	5	465	564	884	N/A	N/A	N/A	N/A	N/A	N/A
	10	467	573	891	N/A	N/A	N/A	N/A	N/A	N/A
	20	490	595	896	N/A	N/A	N/A	N/A	N/A	N/A
	30	472	607	946	N/A	N/A	N/A	N/A	N/A	N/A
PE	5	585	741	777	N/A	N/A	N/A	N/A	N/A	N/A
	10	614	757	805	N/A	N/A	N/A	N/A	N/A	N/A
	20	642	770	805	N/A	N/A	N/A	N/A	N/A	N/A
	30	649	779	819	N/A	N/A	N/A	N/A	N/A	N/A
Dacron	5	593	688	929	N/A	N/A	N/A	929	1148	Incomplete
	10	613	708	952	N/A	N/A	N/A	952	Incomplete	Incomplete
	20	623	724	979	N/A	N/A	N/A	979	Incomplete	Incomplete
	30	633	735	979	N/A	N/A	N/A	979	Incomplete	Incomplete
Rubber	5	447	642	855	N/A	N/A	N/A	855	1173	Incomplete
	10	457	653	877	N/A	N/A	N/A	877	1173	Incomplete
	20	464	669	884	N/A	N/A	N/A	884	1173	Incomplete
	30	473	681	910	N/A	N/A	N/A	910	1173	Incomplete

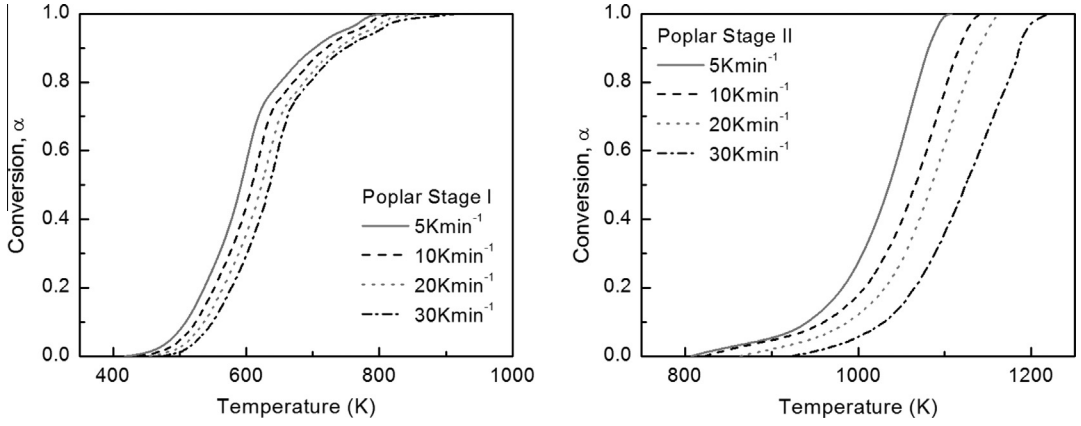

Fig. 3. α vs. temperature curves for the CO_2-gasification of poplar at different heating rates in reaction stages I and II.

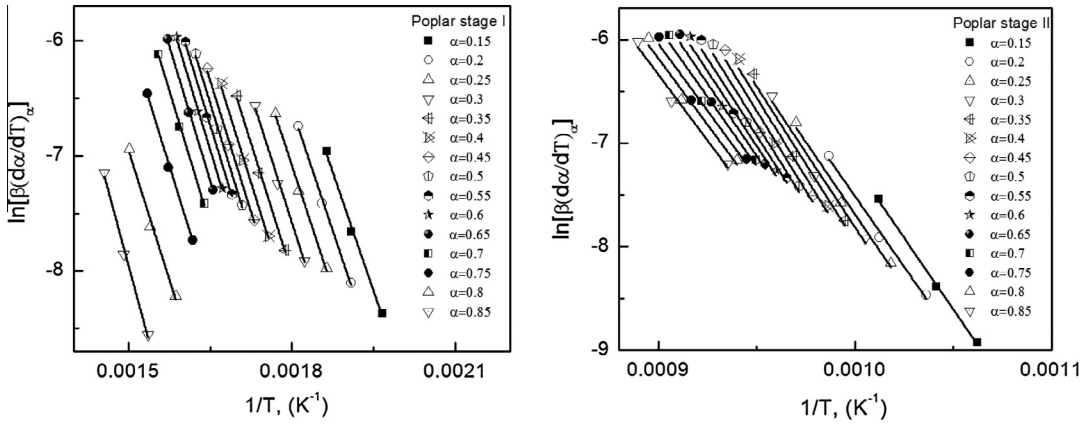

Fig. 4. The Arrhenius plots for the CO_2-gasification of poplar at different reaction stages using the Friedman method.

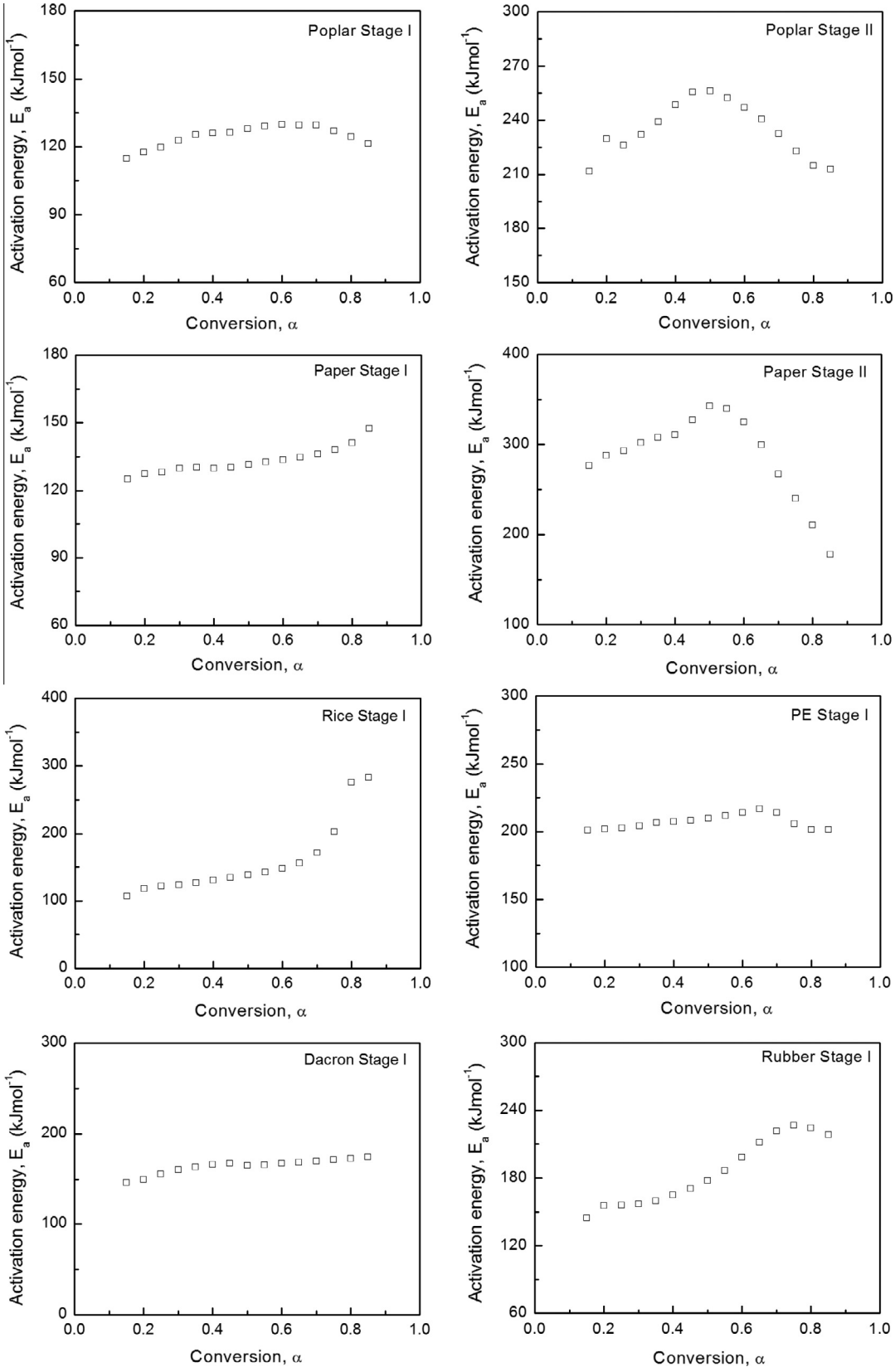

Fig. 5. Plots of activation energy as a function of conversion for the six typical CSW components studied in the present work.

reflected by the increasing activation energy [28]. However, when the conversion was greater than 50%, the reaction may have started to switch from stage II to stage III dominated by the CO_2-gasification of fixed-carbon, resulting in a lower activation energy [23,24,27]. For the other four CSW materials, the activation energies were only available in the pyrolysis stage due to the aforementioned limitation. For synthetic materials, PE and dacron, which were constructed by monomers of simple molecules, the

determined activation energies as a function of the conversion fell into a very narrow range. Therefore, in this pyrolysis reaction stage, the single step reaction assumption can be adopted to describe the thermal decomposition of these two CSW materials and most importantly, the activation energies obtained were independent of the model used and thus can be used for further kinetic analysis. On the other hand, the compositions of the rice and rubber samples were much more complex than those of the two synthetic materials. Therefore, the dependency of the activation energies on the degree of conversion is expected to be strong. The variation in the activation energy of rice and the rubber, as shown in Fig. 5, reveals the complex reaction mechanisms during the gasification process of these two materials. Thus, a multi-step reaction model such as the distributed activation energy model (DAEM) [22,28] should be considered for further kinetic analysis.

4. Conclusions

The pyrolysis in N_2 and CO_2-gasification of six selected typical CSW components were systematically investigated using a TGA operating at varying heating rates to identify the key thermal events during the thermal conversion of the CSW. Three distinctive characteristic reactions stages, namely, the pyrolysis of the raw CSW (stage I), gasification of the char of incomplete carbonisation (stage II) and the gasification of the fixed carbon (stage III), were revealed and described according to their characteristic temperatures of occurrence as the three key thermal events of the gasification of CSW in CO_2. Poplar and paper went through all three stages (stages I, II and III); rubber and dacron incurred two stages (stages I and III; while PE and rice only showed one stage (stage I) reactions during their respective CO_2-gasification process. The pyrolysis process (stage I) of the CSW in CO_2 was similar to that in N_2 but CO_2 shifted the reaction to a higher temperature region. The activation energy as a function of conversion obtained for all the CSW samples using the Friedman method was independent of the reaction models, providing useful information about the complex reaction mechanisms during the gasification process. In stage I, the activation energies of poplar, PE and dacron were constant regardless of the degree of conversion, while the activation energies of paper, rice and rubber increased as the conversion increased. In stage II, the activation energies of both poplar and paper increased first as the reaction progressed but decreased after 50% conversion.

Acknowledgments

Financial and other supports have been received for this research from the National Basic Research Program of China (973 program, Grant 2011CB201502) and the Australian Research Council under the Linkage Projects scheme (ARC LP100200135).

References

[1] Cheng H, Hu Y. Municipal solid waste (MSW) as a renewable source of energy: current and future practices in China. Bioresour Technol 2010;101:3816–24.
[2] Muthuraman M, Namioka T, Yoshikawa K. Characteristics of co-combustion and kinetic study on hydrothermally treated municipal solid waste with different rank coals: a thermogravimetric analysis. Appl Energy 2010;87:141–8.
[3] Duo W, Leclerc D. Thermodynamic analysis and kinetic modelling of dioxin formation and emissions from power boilers firing salt-laden hog fuel. Chemosphere 2007;67:164–76.
[4] Ohmukai Y, Hasegawa I, Mae K. Pyrolysis of the mixture of biomass and plastics in countercurrent flow reactor Part I: Experimental analysis and modeling of kinetics. Fuel 2008;87:3105–11.
[5] Lai Z, Ma X, Tang Y, Lin H. Thermogravimetric analysis of the thermal decomposition of MSW in N_2, CO_2 and CO_2/N_2 atmospheres. Fuel Process Technol 2012;102:18–23.
[6] Vassura I, Passarini F, Ferroni L, Bernardi E, Morselli L. PCDD/Fs atmospheric deposition fluxes and soil contamination close to a municipal solid waste incinerator. Chemosphere 2011;83:1366–73.
[7] Stanmore BR. The formation of dioxins in combustion systems. Combust Flame 2004;136:398–427.
[8] Altarawneh M, Dlugogorski BZ, Kennedy EM, Mackie JC. Mechanisms for formation, chlorination, dechlorination and destruction of polychlorinated dibenzo-p-dioxins and dibenzofurans (PCDD/Fs). Prog Energy Combust Sci 2009;35:245–74.
[9] Arena U. Process and technological aspects of municipal solid waste gasification. Waste Manage 2012;32:625–39.
[10] He M, Hu Z, Xiao B, Li J, Guo X, Luo S, et al. Hydrogen-rich gas from catalytic steam gasification of municipal solid waste (MSW): influence of catalyst and temperature on yield and product composition. Int J Hydrogen Energy 2009;34:195–203.
[11] He M, Xiao B, Hu Z, Liu S, Guo X, Luo S. Syngas production from catalytic gasification of waste polyethylene: influence of temperature on gas yield and composition. Int J Hydrogen Energy 2009;34:1342–8.
[12] Sanchez ME, Otero M, Gómez X, Morán A. Thermogravimetric kinetic analysis of the combustion of biowastes. Renew Energy 2009;34:1622–7.
[13] Liu GH, Ma XQ, Yu Z. Experimental and kinetic modeling of oxygen-enriched air combustion of municipal solid waste. Waste Manage 2009;29:792–6.
[14] Łabojko G, Kotyczka-Morańska M, Plis A, Ściążko M. Kinetic study of polish hard coal and its char gasification using carbon dioxide. Thermochim Acta 2012;549:158–65.
[15] Chen TJ, Wu C, Liu RH, Fei WT, Liu SY. Effect of hot vapor filtration on the characterization of bio-oil from rice husks with fast pyrolysis in a fluidized-bed reactor. Bioresour Technol 2011;102:6178–85.
[16] Chen TJ, Deng CJ, Liu RH. Effect of selective condensation on the characterization of bio-oil from pine sawdust fast pyrolysis using a fluidized-bed reactor. Energy Fuels 2010;24:6616–23.
[17] Shen L, Zhang DK. Low-temperature pyrolysis of sewage sludge and putrescible garbage for fuel oil production. Fuel 2005;84:809–15.
[18] Shen L, Zhang DK. An experimental study of oil recovery from sewage sludge by low-temperature pyrolysis in a fluidised-bed. Fuel 2003;82:465–72.
[19] Friedman HL. Kinetics of thermal degradation of char-forming plastics from thermogravimetry. Application to a phenolic plastic. J Polym Sci C: Polym Sympos 1964;6:183–95.
[20] Simmons GM, Gentry M. Particle size limitations due to heat transfer in determining pyrolysis kinetics of biomass. J Anal Appl Pyrol 1986;10:117–27.
[21] Wu WX, Cai JM, Liu RH. Isoconversional kinetic analysis of distributed activation energy model processes for pyrolysis of solid fuels. Ind Eng Chem Res 2013;52:14376–83.
[22] Cai JM, Liu RH. New distributed activation energy model: numerical solution and application to pyrolysis kinetics of some types of biomass. Bioresour Technol 2008;99:2795–9.
[23] Slopiecka K, Bartocci P, Fantozzi F. Thermogravimetric analysis and kinetic study of poplar wood pyrolysis. Appl Energy 2012;97:491–7.
[24] Vamvuka D, Kakaras E, Kastanaki E, Grammelis P. Pyrolysis characteristics and kinetics of biomass residuals mixtures with lignite. Fuel 2003;82:1949–60.
[25] Vyazovkin S, Burnham AK, Criado JM, Pérez-Maqueda LA, Popescu C, Sbirrazzuoli N. ICTAC kinetics committee recommendations for performing kinetic computations on thermal analysis data. Thermochim Acta 2011;520:1–19.
[26] Zhu MM, Zhou WX, Zhang ZZ, Li JB, Zhang DK. Effect of temperature on pyrolysis products of a pine sawdust in an indirectly fired rotary kiln. Chemeca 2013, Brisbane, 2013.
[27] Chen TJ, Wu JL, Zhang JZ, Wu JH, Sun L. Gasification kinetic analysis of the three pseudocomponents of biomass-cellulose, semicellulose and lignin. Bioresour Technol 2014;153:223–9.
[28] Cai JM, Wu WX, Liu RH. Sensitivity analysis of three-parallel-DAEM-reaction model for describing rice straw pyrolysis. Bioresour Technol 2013;132:423–6.